

11-1-2023

Analytical prediction of stress and strain in adhesive tube-to-tube joints under thermal expansion/contraction

H. Liu

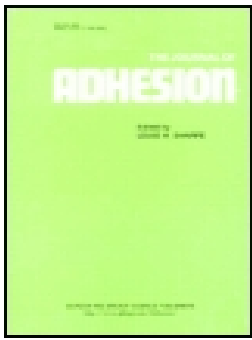
Justin A. Weibel
jaweibel@purdue.edu

E A. Groll

Follow this and additional works at: <https://docs.lib.purdue.edu/coolingpubs>

Liu, H.; Weibel, Justin A.; and Groll, E A., "Analytical prediction of stress and strain in adhesive tube-to-tube joints under thermal expansion/contraction" (2023). *CTRC Research Publications*. Paper 411.
<http://dx.doi.org/https://doi.org/10.1080/00218464.2023.2178307>

This document has been made available through Purdue e-Pubs, a service of the Purdue University Libraries.
Please contact epubs@purdue.edu for additional information.




Analytical prediction of stress and strain in adhesive tube-to-tube joints under thermal expansion/contraction

Haotian Liu, Justin A. Weibel & Eckhard A. Groll


To cite this article: Haotian Liu, Justin A. Weibel & Eckhard A. Groll (2023): Analytical prediction of stress and strain in adhesive tube-to-tube joints under thermal expansion/contraction, The Journal of Adhesion, DOI: [10.1080/00218464.2023.2178307](https://doi.org/10.1080/00218464.2023.2178307)


To link to this article: <https://doi.org/10.1080/00218464.2023.2178307>

 View supplementary material [↗](#)

 Published online: 16 Feb 2023.

 Submit your article to this journal [↗](#)

 Article views: 26

 View related articles [↗](#)

 View Crossmark data [↗](#)



Analytical prediction of stress and strain in adhesive tube-to-tube joints under thermal expansion/contraction

Haotian Liu^a, Justin A. Weibel^b, and Eckhard A. Groll^a

^aSchool of Mechanical Engineering, Purdue University, Ray W. Herrick Laboratories, West Lafayette, Indiana, USA; ^bSchool of Mechanical Engineering, Purdue University, West Lafayette, Indiana, USA

ABSTRACT

Adhesive joints are widely applied and studied for various industrial applications. The interest in adhesive joints has expanded to include heating, ventilation, air conditioning, and refrigeration (HVAC&R) systems having a significant number of joints employed for manufacturing. This study investigates an analytical modeling approach for predicting joint stress and strain distribution under static loading with thermal strain. A review of modeling techniques identified the need to develop a joint analytical model under loading conditions representative of HVAC&R applications. The details of the model, governing equations, assumptions, boundary conditions, and solution techniques are first reported. The model is validated via comparison to existing results before performing parametric studies to provide insights on the influences of thermal expansion and inner tube pressure on possible failure. It is found that the joint overlap length plays an important role in stress distribution, while the adhesive thickness has less impact. Overall, the results indicate that static loading failure is not likely a concern for joints in HVAC&R systems, but the thermal strain and stress induced by temperature fluctuations must be carefully considered. This modeling effort establishes a framework that can be used to generate criteria and instructions on designing adhesive joints across different HVAC&R

ARTICLE HISTORY

Received 11 November 2022
Accepted 4 February 2023


KEYWORDS

Analytical modeling; thermal stress; joint design

1. Introduction

In heating, ventilation, air conditioning, and refrigeration (HVAC&R) systems, a large number of tube-to-tube joints are used in manufacturing and assembly processes. Recently, there has been an increased interest in finding alternative joining techniques to ease the installation of complex vapor compression systems, such as supermarket refrigeration or variable refrigerant flow (VRV) air conditioning systems. This interest is heightened by the use of potentially flammable or mildly flammable alternate refrigerants that are more efficient and environmentally friendly. Adhesive tube-to-tube joints have potential energy and cost saving benefits compared to brazing, with

CONTACT Haotian Liu  liu1460@purdue.edu  School of Mechanical Engineering, Purdue University, Ray W. Herrick Laboratories, West Lafayette, Indiana, USA

 Supplemental data for this article can be accessed online at <https://doi.org/10.1080/00218464.2023.2178307>

© 2023 Taylor & Francis Group, LLC

additional advantages including freedom in design and safe field installation with flammable refrigerants. However, the reliability of adhesive joints under loading conditions representative of HVAC&R systems has not been thoroughly studied. Considering the diversity of operating conditions and applications that HVAC&R systems present, it is very challenging to build physical test stands to explore all possible adhesive joint geometries and boundary conditions. Modeling tools are necessary to simulate their performance and potential failure.

Adhesive joint modeling tools are typically built with inputs being the known properties of the adhesive, as provided by the manufacturer. Due to the wide use of structural adhesive joints across many applications, prediction of adhesive joint strength, stress distribution, and failure has drawn massive attention over the decades. Given the variety of different joint geometries, many different modeling and solution methods are provided in the literature. Stress and strain predictions are most commonly used to investigate the joint safety and reliability. These analyses examine the equilibrium of the joints with stress–strain and compatibility equations. Solving the set of governing equations thereby developed can be done either analytically or numerically; both techniques are reviewed in the following discussion. The specific scope and novelty of the current study is to build a comprehensive model for tube-to-tube joint geometries where not only the static loading is considered, but also the effect of thermal expansion under a temperature change. The developed model can thereby provide the basis for the design of the new adhesive joints, formulating equivalent strength limits, and predicting the failure of the joints. The model can also be used to design new adhesive joints and new fittings, as well as to optimize the geometry for different size fittings.

Adhesively bonded tube-to-tube joints are commonly encountered in engineering applications, and there are several seminal structural analyses considering different loading conditions, assumptions, and geometries. One of the earliest models for tube-to-tube joints was developed by Lubkin and Reissner.^[1] However, over the past several decades since, research on tube-to-tube joints in the technical literature is considerably less compared to planar geometries such as single- or double-lap joints.^[2]

Several analytical models have been developed to predict the normal and shear stress distributions in the adhesive layer of tube-to-tube joints under various loading conditions. Lubkin and Reissner^[1] studied joints under axial loading only, considering an axisymmetric configuration with several assumptions used for flat single lap joints. The governing differential equations were then constructed using equilibrium equations and stress–strain relations. Results were reported in terms of normalized shear and peel stresses for various specific cases with no explicit solution provided. Terekhova and Skoryi^[3] and Pugno and Carpinteri^[4] used similar approaches and assumptions as Lubkin and Reissner^[1] to further study the effects of internal pressure

and the variation of tube cross-sections, respectively. Shi and Cheng^[5] proposed a different model that considered thick-tube walls (adherends), also under axial loading only, providing a wider range of applications. The model was built in cylindrical coordinates using the equilibrium equation and compatibility equations. A closed-form solution was not explicitly reported, but two numerical results were given.

Considering the effect of adhesive thickness further complicates the predictions. Nayeb-Hashemi et al.^[6] investigated the behavior of tube-to-tube joints under axial and torsional loadings and considered the variation of shear stress across the adhesive thickness. Nemeş et al.^[7] and Nemeş and Lachaud^[8] proposed a model considering a complex stress state with non-isotropic behavior of the tubes. The shear and hoop stresses in the tubes were both variables over the thickness, within both the tubes and adhesives. The authors conducted parametric studies and reported how the stresses changed with varying overlap length, thickness, and material properties, but no analytical solution was given. Furthermore, Kumar,^[9] Kumar and Scanlan,^[10] and Martinez et al.^[11] developed models on the same basis to study different formulations and geometries. There are several additional studies that have contributed to the literature on analytical modeling of tube-to-tube joints, each with similar modeling approaches or loading conditions as those summarized above.^[12–16]

Another powerful and common tool in predicting the stress field is the finite element method (FEM), which has been developed to study various adhesive-bonded joints.^[17,18] FEM is a numerical method often applied in engineering situations that involve boundary value problems for partial differential equations that are otherwise hard to solve analytically. Alwar and Nagaraja^[19] used FEM to analyze the stresses in tube-to-tube single lap joints subjected to torsion. The time-dependent properties of the adhesive are taken into account by assuming that the adhesive is viscoelastic. Yadagiri et al.^[20] also studied the viscoelastic analysis of adhesively bonded joints using FEM. Adams and Peppiatt^[21] used FEM to calculate the stresses in an adhesive-bonded tube-to-tube single lap joint subjected to both axial and torsional loads using axisymmetric quadratic isoparametric finite elements. The axial loading results were compared with the published closed-form solution from Lubkin and Reissner.^[1] Goglio and Paolino^[2] performed a critical review and assessment of the published finite element models for predicting stress distributions in adhesive tube-to-tube joints under axial loading and concluded that all the models predicted the shear stress correctly, but only the Lubkin and Reissner^[1] solution predicted the correct peel stress distribution.

Although significant progress has been made in the development of models to predict stress and strain in adhesively bonded tube-to-tube joints, an approach that focuses on the typical joint geometry and operating conditions within HVAC&R systems is still lacking. Most of the previous work has

focused on studying the axial or torsional loading, few have considered internal pressure, and none has considered the practical combination of static loading with thermal expansion. In order to predict stress and strain under these conditions, both analytical approaches and numerical methods must be considered.

Analytical approaches require simplifying assumptions to reduce the complexity such that the formulated differential equation set can be solved, while numerical methods (FEM) provide an approximate estimate of the exact solution. In FEM, it is routinely noted that inconsistency in finite element results is observed due to overly coarse meshes, driven by the high computational cost. The element type and mesh size need to be carefully selected, as discussed by Adams and Peppiatt.^[22] In analytical approaches, many of them do not result in closed-form solutions (or they are not provided). However, analytical solutions are most valuable in providing insight into the stress and strain fields. By examining the form of the solution, the relation between the stresses and inputs such as geometric sizes, material properties, and loading conditions can be more intuitively identified. With the stresses and strains available, a subsequent fatigue evaluation can also be processed. Finally, compared to numerical approaches, the low computational cost of analytical approaches allows broad exploration of the design space with different inputs, which can be used to formally optimize or provide design guidance with a short turnaround.

Because the goal of the current effort is to better understand the behavior of the tube-to-tube joints and provide guidance on design, optimization, and reliability analysis, an analytical modeling approach is adopted. In particular, as pointed out by Goglio and Paolino,^[23] the Lubkin and Reissner^[1] model predicts both peel stress and shear stress accurately within the adhesive layer under the axial loading condition compared with FEM. Thus, this model is taken as a starting point and adapted to the more complicated boundary and loading conditions as experienced in HVAC&R systems.

2. Model formulation

2.1. Geometry, material, and loading condition

In HVAC&R applications, the joint connecting the two tubes uses either a female-to-female coupling or an expanded female tube end. In either case, the gap to the female tube diameter determines the adhesive layer thickness. [Figure 1](#) shows a detailed schematic of the tube-to-tube joint region with the main geometric parameters and material properties labelled. In order to keep the model setup more general, the two adherends are allowed to have different materials denoted by subscripts 1 and 2 (e.g., r_1 and r_2 are the radii of the two tubes at the midpoint; E_1 and E_2 are the Young's moduli; and ν_1 and ν_2 are the

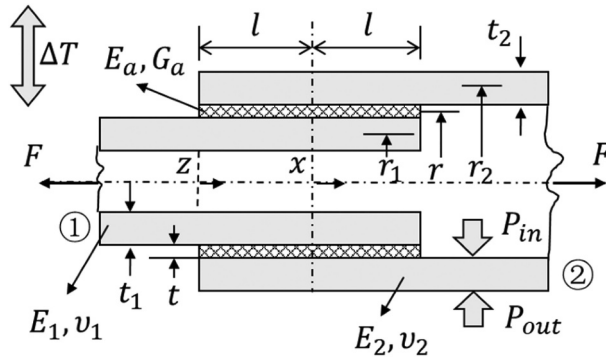


Figure 1. Schematic diagram of the tube-to-tube joint with the key geometric variables and material properties labelled.

Poisson's ratios). The adhesive is the shaded region in between the tubes, where r is the radius at the midpoint of the adhesive, E_a is the Young's modulus, and G_a is the shear modulus of the adhesive. The overlap area as well as the adhesive length is $2l$. The axial coordinate x is set to start at the center of the adhesive overlap region. A normalized coordinate z is defined to start at the left end.

The possible loading conditions are also specified in the most general possible setup. The axial force loading the joint is F and no torsion loading is applied. The tube has internal pressure of P_{in} and outside pressure P_{out} (usually atmospheric pressure). The temperature swing imposed for purposes of evaluating the effects of thermal expansion is indicated as ΔT .

Before introducing the forces and stresses, several important assumptions are discussed. The tubes are modeled as thin shells subjected to axial tension, shear force, and bending moments. Both tubes have axial displacement, radial displacement, and rotation. The adhesive is treated as an elastic medium as a spring layer with shear stresses and peel stresses; the axial stress σ_x is assumed negligible. The adhesive layer is thin such that the stresses are constant over the thickness and varying along the axial direction only. There is no circumferential shear stress because no torsion is applied to the joints. The forces, stresses, and strains should be axisymmetric due to the axisymmetric geometry. In addition, as indicated by Lubkin and Reissner,^[1] the model developed is representative of stresses in the mid-thickness of adhesives. Note that it has been shown that the out-of-plane stresses are slightly higher at the interface between the adhesive and substrates.

A 3D view of a section of a single tube, with detailed forces and stresses labelled, and the elementary-free body diagrams of the joints are shown in Figure 2. In the tubes, the forces per unit length can be grouped into the axial (T_1 , T_2), transverse (V_1 , V_2), hoop (N_1 , N_2) directions, and the bending moments per unit length are (M_1 , M_2). In the adhesive layer, there are two

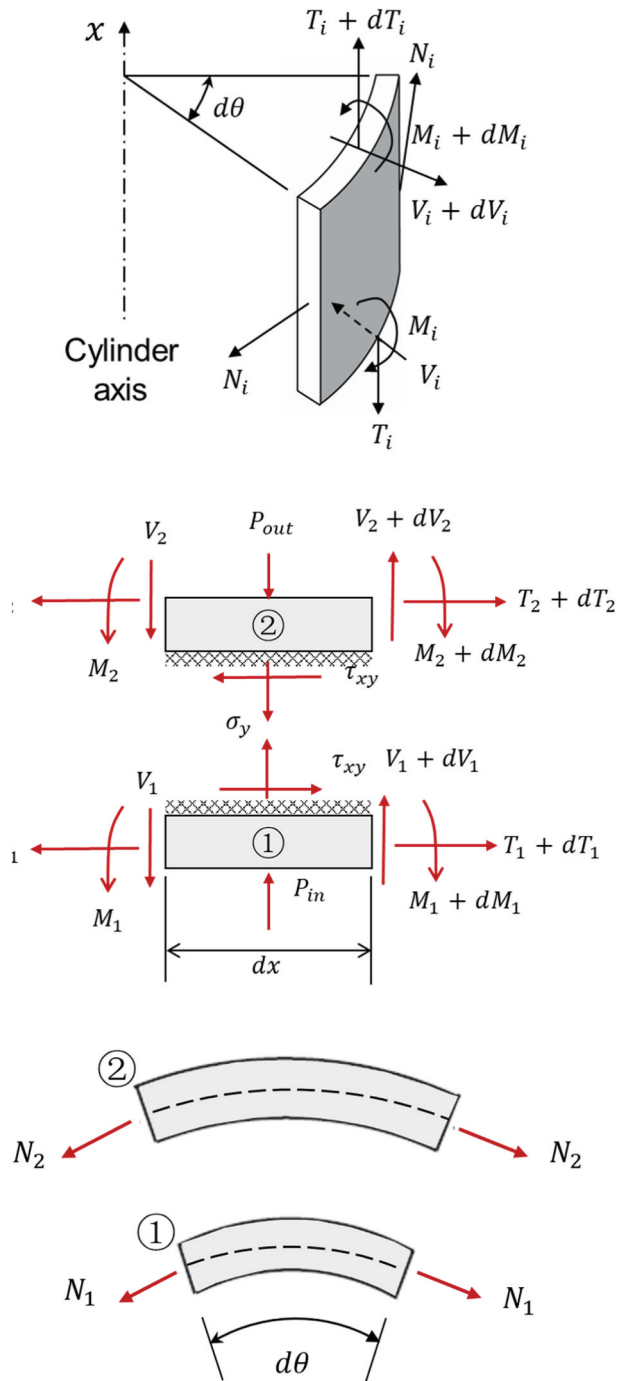


Figure 2. 3D view of a section of the tube with forces and elementary free body diagrams of the joint with forces and stresses labelled.

stresses considered, peel σ_y and shear τ_{xy} . Note that due to the axisymmetric geometry, any derivative in the circumferential direction will be zero.

2.2. Governing equations

The equilibrium stress–strain relations are examined in this section to form a set of governing equations to model the joint.

The axial equilibrium in adherend 1 can be written as:

$$r_1 \frac{dT_1}{dx} + r\tau_{xy} = 0 \quad (1)$$

For adherend 2 the axial equilibrium simplifies similarly, noting that the shear stress has an opposite sign compared to adherend 1:

$$r_2 \frac{dT_2}{dx} - r\tau_{xy} = 0 \quad (2)$$

The transverse equilibrium for adherend 1 is:

$$r_1 \frac{dV_1}{dx} + r\sigma_y + P_{in}r_1 - N_1 = 0 \quad (3)$$

For adherend 2 the transverse equilibrium simplifies similarly, noting that the pressure and the peel stresses in the adhesive have opposite signs compared to adherend 1:

$$r_2 \frac{dV_2}{dx} - r\sigma_y - P_{out}r_2 - N_2 = 0 \quad (4)$$

The moment balances for both tubes can be written and simplify in a similar fashion:

$$(M_1 + dM_1)r_1d\theta + \tau_{xy}r dx d\theta \frac{t_1}{2} = M_1r_1d\theta + V_1r_1 dx d\theta \quad (5)$$

$$r_1 \frac{dM_1}{dx} - r_1V_1 + r \frac{t_1}{2} \tau_{xy} = 0 \quad (6)$$

$$r_2 \frac{dM_2}{dx} - r_2V_2 + r \frac{t_2}{2} \tau_{xy} = 0 \quad (7)$$

The strain and displacement relations of each adherend can be calculated as:

$$\varepsilon_x = \frac{(du + dx) - dx}{dx} = \frac{du}{dx} \quad (8)$$

$$\varepsilon_\theta = \frac{(r + v)d\theta - rd\theta}{rd\theta} = \frac{v}{r} \quad (9)$$

As mentioned earlier, due to the axisymmetric geometry, the circumferential displacement and strain is zero. The stress–strain relation is given here to consider the axial, hoop, and bending deformation. The longitudinal displacement (u_1, u_2) and transverse displacement (v_1, v_2) can be written in terms of the force and thermal strain:

$$\varepsilon_{x1} = \frac{du_1}{dx} = \frac{T_1 - v_1 N_1}{E_1 t_1} + \alpha_1 T \quad (10)$$

$$\varepsilon_{x2} = \frac{du_2}{dx} = \frac{T_2 - v_2 N_2}{E_2 t_2} + \alpha_2 T \quad (11)$$

$$\varepsilon_{\theta 2} = \frac{v_2}{r_2} = \frac{N_2 - v_2 T_2}{E_2 t_2} + \alpha_2 T \quad (12)$$

$$\varepsilon_{\theta 1} = \frac{v_1}{r_1} = \frac{N_1 - v_1 T_1}{E_1 t_1} + \alpha_1 T \quad (13)$$

where α_1 and α_2 are the thermal expansion coefficients of the adherends 1 and 2. Note that in this model, the temperature change ΔT is considered uniform for the entire assembly. The transient process of heat transfer from the fluid to the environment, and the resulting temperature gradient within the joints, is not considered due to the high thermal conductivity and small thermal mass.

The bending deformation can be written as:

$$\frac{d^2 v_1}{dx^2} = -\frac{M_1}{D_1} \text{ and } \frac{d^2 v_2}{dx^2} = -\frac{M_2}{D_2} \quad (14)$$

where D_i is the bending stiffness for the corresponding adherend:

$$D_i = \frac{E_i t_i^3}{12(1 - \nu_i^2)}, i = 1, 2 \quad (15)$$

The adhesive layer is treated to have both normal stress σ_y and shear stress τ_{xy} . It is usually a very thin layer, and thus, bending of the adhesive is not considered. It is also assumed that the adhesive follows a stress–strain relation with linear elasticity.

$$\sigma_y = \frac{E_a}{t} (v_2 - v_1) \quad (16)$$

$$\tau_{xy} = \frac{G_a}{t} (u_{2,in} - u_{1,out}) \quad (17)$$

The surface displacements must coincide with those at the midpoint to ensure the continuity of the solid for the displacement at the outer diameter of tube 1 and at the inner diameter of tube 2:

$$u_{1,out} = u_1 - \left(\frac{dv_1}{dx}\right)\left(\frac{t_1}{2}\right) \quad (18)$$

$$u_{2,in} = u_2 + \left(\frac{dv_2}{dx}\right)\left(\frac{t_2}{2}\right) \quad (19)$$

A summary of all the known and unknown parameters are listed below:

- Knowns:
 - Geometric parameters: r_1, r_2, r, t_1, t_2, t
 - Boundary forces and pressures: P_{in}, P_{out}, F
 - Material properties: $E_1, E_2, v_1, v_2, \alpha$
 - Temperature change: ΔT
- Unknowns:
 - Stresses: τ_{xy}, σ_y
 - Force terms: $T_1, T_2, V_1, V_2, N_1, N_2, M_1, M_2$
 - Displacement/strain terms: $u_1, u_2, v_1, v_2, u_{1,out}, u_{2,in}$

There are equal number (16) of equations (1), (2), (3), (4), (6), (7), (10), (11), (12), (13), (14), (16), (17), (18), and (19) and unknown variables with all the variables as a function of the x coordinate. Hence, the problem can then be solved with proper boundary conditions. Moreover, the global axial equilibrium for the joints under the axial force F can be written as:

$$2\pi(r_1T_1 + r_2T_2) = F \quad (20)$$

For solving purposes, an auxiliary unknown T_0 is introduced to satisfy:

$$rT_0 = r_2T_2 - r_1T_1 \quad (21)$$

Combined with Eqns. (1) and (2):

$$\frac{dT_0}{dx} = 2\tau_{xy} \quad (22)$$

In the simplification, τ_{xy} is replaced with $\frac{dT_0}{dx}$ to reduce the order of the differential equation. The mathematical manipulations and variable elimination procedure, detailed in the Supplementary Material section S1, leads to the following set of three simultaneous differential equations (23), (24) and (25) with three unknowns v_1, v_2 and T_0 . With appropriate boundary conditions, this set can be solved to then further solve for the stress and strain fields in the joint.

$$\begin{aligned} \frac{d^4v_1}{dx^4} + 12(1-v_1^2)\left(\frac{1}{r_1^2t_1^2} + \frac{rE_a}{E_1t_1^3r_1t}\right)v_1 - 12(1-v_1^2)\frac{rE_a}{E_1t_1^3r_1t}v_2 - 3\frac{(1-v_1^2)r}{E_1t_1^2r_1}\frac{d^2T_0}{dx^2} \\ - 6\frac{(1-v_1^2)rv_1}{E_1t_1^3r_1}T_0 = -\left(\frac{Fv_1}{4\pi r_1^2} + \frac{E_1t_1\alpha_1}{r_1}\Delta T - P_{in}\right)\left(\frac{12(1-v_1^2)}{E_1t_1^3}\right) \end{aligned} \quad (23)$$

$$\begin{aligned} & \frac{d^4 v_2}{dx^4} + 12(1-v_2^2) \left(\frac{1}{r_2^2 t_2^2} + \frac{rE_a}{E_2 t_2^3 r_2 t} \right) v_2 - 12(1-v_2^2) \frac{rE_a}{E_2 t_2^3 r_2 t} v_1 - 3 \frac{(1-v_2^2)r}{E_2 t_2^2 r_2} \frac{d^2 T_0}{dx^2} \\ & + 6 \frac{(1-v_2^2)rv_1}{E_2 t_2^3 r_2^2} T_0 = - \left(\frac{Fv_2}{4\pi r_2^2} + \frac{E_2 t_2 \alpha_2}{r_2} \Delta T + P_{out} \right) \left(\frac{12(1-v_2^2)}{E_2 t_2^3} \right) \end{aligned} \quad (24)$$

$$\begin{aligned} & \frac{d^2 T_0}{dx^2} - \frac{G_a r}{t} \left(\frac{(1-v_1^2)}{E_1 r_1 t_1} + \frac{(1-v_2^2)}{E_2 r_2 t_2} \right) T_0 - \frac{G_a}{t} \left(t_1 \frac{d^2 v_1}{dx^2} + t_2 \frac{d^2 v_2}{dx^2} \right) - \frac{2G_a v_1}{tr_1} v_1 + \frac{2G_a v_2}{tr_2} v_2 \\ & = \frac{2G_a}{t} \left(-\frac{F(1-v^2)}{4\pi r_1 E_1 t_1} + \frac{F(1-v^2)}{4\pi r_2 E_2 t_2} - (1-v_1)\alpha_1 \Delta T + (1-v_2)\alpha_2 \Delta T \right) \end{aligned} \quad (25)$$

2.3. Boundary conditions

The differential equations must be solved under appropriate boundary conditions. In HVAC&R systems, the joints at different locations may have different boundary conditions. The following boundary conditions therefore reflect the most common scenario for joints to seal and connect two tubes without significant axial force and torsion.

As shown in [Figure 1](#), where the tube and adhesive layer both end, it is evident that the forces and moments must disappear:

$$\begin{aligned} & \text{at } x = -l, \quad T_2 = V_2 = M_2 = 0 \\ & \text{at } x = l, \quad T_1 = V_1 = M_1 = 0 \end{aligned} \quad (26)$$

In the section where the adhesive layer ends but the tube continues, the tubes are subjected to bending and shear. The boundary conditions for tubes at this transition between the overlapping and non-overlapping areas are not simple axial loads and must be found by ensuring the continuity of force, moment, displacement, and rotation. As discussed in Goglio and Paolino (2014), the results can be derived by deleting the terms related to the adhesive layers or by referring to the theory for thin-cylinder shells with bending (Coates, 1930):

$$v_{1,tube} = e^{\lambda_1 x} (A_{v1} \cos \lambda_1 x + B_{v1} \sin \lambda_1 x) - \frac{v_1 F}{2\pi E_1 t_1} \quad (27)$$

$$v_{2,tube} = e^{-\lambda_2 x} (A_{v2} \cos \lambda_2 x + B_{v2} \sin \lambda_2 x) - \frac{v_2 F}{2\pi E_2 t_2} \quad (28)$$

where $\lambda_i^4 = \frac{3(1-v_i^2)}{r_i^2 t_i^2}$ and A_{vi}, B_{vi} are constants to be determined.

The continuity of force, moment, displacement, and rotation at both ends of the joints can be written as:

$$\begin{aligned}
 \text{Force: } & V_{1,tube}|_{x=-l} = V_1|x=-l; \quad V_{2,tube}|_{x=l} = V_2|x=l; \\
 \text{Moment: } & M_{1,tube}|_{x=-l} = M_1|x=-l; \quad M_{2,tube}|_{x=l} = M_2|x=l; \\
 \text{Displacement: } & v_{1,tube}|_{x=-l} = v_1|x=-l; \quad v_{2,tube}|_{x=l} = v_2|x=l; \quad (29) \\
 \text{Rotation: } & \frac{dv_{1,tube}}{dx}|_{x=-l} = \frac{dv_1}{dx}|_{x=-l}; \quad \frac{dv_{2,tube}}{dx}|_{x=l} = \frac{dv_2}{dx}|_{x=l};
 \end{aligned}$$

where $V_{i,tube} = -D_i \frac{d^3 v_i}{dx^3}$, $M_{i,tube} = -D_i \frac{d^2 v_i}{dx^2}$ and $D_i = \frac{E_i t_i^3}{12(1-\nu_i^2)}$ ($i = 1, 2$).

2.4. Solution method

The original study by Lubkin and Reissner^[1] provides no details on the solution procedure beyond a remark that the equation set is linear with constant coefficients and thus can be solved with standard methods. Nevertheless, in the pursuit of an explicit closed-form solution, the high order of the set of differential equations is a major practical difficulty. While it is possible to achieve approximate solutions without particular difficulty by numerical integration, we seek an analytical solution as discussed in the introduction. Goglio and Paolino^[23] revisit the Lubkin and Reissner^[1] model and provide a solution method using Laplace transforms. A similar solution approach using Laplace transforms is applied in this study, but the procedure of finding the partial fraction decomposition is modified to simplify the calculation. The solution process is evaluated using Mathematica. The algorithm used to solve the set of governing equations is shown in Figure 3, where $f(z)$, $g(z)$, and $h(z)$ are three dimensionless functions and $z = (x + l)/2l$ is a dimensionless variable such that $z = 0$ ($x = -l$) at the left end of the adhesive and $z = 1$ ($x = l$) at the right end of the adhesive. The detailed expressions of the dimensionless functions and their functions can be found in the Supplementary Material section S2.

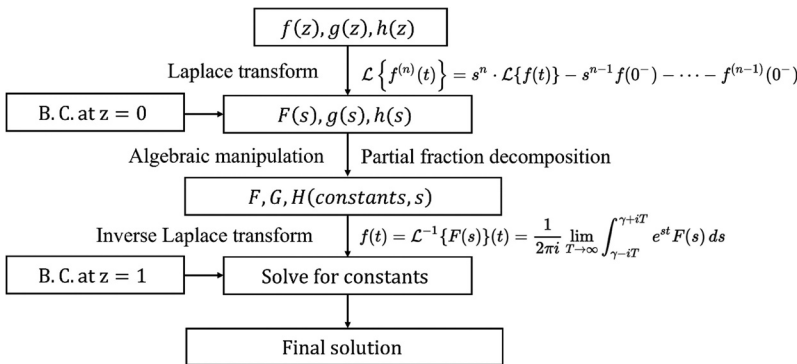


Figure 3. Flow chart of the solution algorithm using Laplace transforms with boundary conditions.

The final closed-form solution is summarized as follows with the detailed steps that are reported in the Supplementary Material section S2.

$$\begin{aligned}\sigma_y(z) &= \frac{F}{2\pi r} \frac{E_a}{G_a} \left(\frac{B_2^2}{t_2} \frac{n_{2,0}}{d_0} - \frac{B_1^2}{t_1} \frac{n_{1,0}}{d_0} \right) + \frac{F}{4\pi r l} \frac{E_a}{G_a} \sum_{i=1}^3 (\cosh(r_j z) \times (c_{\sigma,i,1} \cos(m_i z) \\ &+ c_{\sigma,i,2} \sin(m_i z)) + \sinh(r_i z) \times (c_{\sigma,i,3} \cos(m_i z) + c_{\sigma,i,4} \sin(m_j z))) \\ \tau_{xy}(z) &= \frac{F}{8\pi r l} \sum_{i=1}^3 (\cosh(r_j z) \times (c_{\tau,i,1} \cos(m_i z) + c_{\tau,i,2} \sin(m_i z)) + \sinh(r_i z) \\ &\times (c_{\tau,i,3} \cos(m_i z) + c_{\tau,i,4} \sin(m_j z)))\end{aligned}\quad (30)$$

where r_i and m_i are defined based on the non-zero roots defined in equations (S37) in the Supplementary Material and the rest of the coefficients can be expressed as:

$$\begin{aligned}c_{\sigma,i,j} &= B_2^2 \frac{2l}{t_2} c_{i,j,2} - B_1^2 \frac{2l}{t_2} c_{i,j,2} \quad i = 1, 2, 3 \\ c_{\tau,2k-1,j} &= r_i c_{i,2k-1,3} + m_i c_{i,2k,3} \quad j = 1, 2, 3, 4 \\ c_{\tau,2k,j} &= r_i c_{i,2k+1,3} - m_i c_{i,2k-1,3} \quad k = 1, 2\end{aligned}\quad (31)$$

3. Results and discussion

3.1. Model validation

The model developed here is based on the previous model by Lubkin and Reissner,^[1] but with the additional consideration of the effects of pressure and thermal expansion. Goglio and Paolino^[23] revisited the model of Lubkin and Reissner^[1] to develop an explicit closed-form solution and analyzed the same loading condition with finite element analysis. They compared the original solution of Lubkin and Reissner,^[1] their explicit closed-form analytical solution, and the finite element analysis solution and concluded that all three solutions are consistent.

In this study, the solution method also uses Laplace transforms, as suggested by Goglio and Paolino.^[23] In order to validate the implementation of the current model and its solution method, a validation case using the same loading condition as reported in the literature is considered here. Note that in the validation case, an externally axial force is given without considering the effects of pressure and thermal expansion. The geometric parameters, material properties, and axial loading for the validation cases are reported in Table 1, which were first studied by Lubkin and Reissner^[1] and then reproduced by Goglio and Paolino^[23] with numerical values reported for the solution. Note

Table 1. Geometric sizes, material properties, and loading conditions of the validation case from the literature^[2].

Parameters	r_1 (mm)	r_2 (mm)	r (mm)	t (mm)	t_1 (mm)	t_2 (mm)	l (mm)
Values	48.75	51.25	50	0.25	2.5	2.5	12.5
Parameters	E_1 (GPa)	E_2 (GPa)	ν_1 (-)	ν_2 (-)	E_a (MPa)	G_a (MPa)	F (N)
Values	200	200	0.3	0.3	1000	375	7854

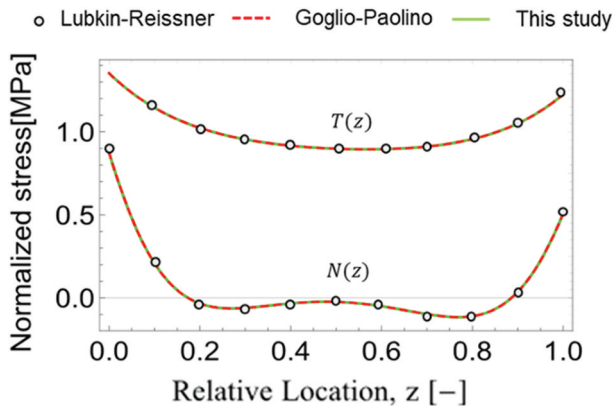
Table 2. Comparison of the numerical values of the initial conditions at $z = 0$ of the reported data in the literature with the model in this study.

Parameters	f_0	f_0^l	g_0	g_0^l	h_0^l
Dragoni and Goglio ^[2]	0.00459	0.02978	0.02384	-0.17159	2.70675
Solver in this study	0.0045952	0.0297451	0.0238371	-0.171582	2.7068

that in Dragoni and Goglio,^[2] the geometric parameters for $r_1 = 48.625\text{mm}$ and $r_2 = 51.375\text{mm}$ do not match with the numerical values reported in the later validation details. After back-calculation using the results, the values are corrected to $r_1 = 48.75\text{mm}$, $r_2 = 51.25\text{mm}$, as shown in Table 1.

The validation is done by first comparing the key resulting numerical values as shown in Table 2. The same values for the initial boundary conditions (write symbols here), as well as the coefficients for the final solution (write symbols here), are achieved with extremely minimal error attributed to the number of significant figures used in the calculation process.

For further verification, an overlay of the normalized stress predictions is plotted in Figure 4. As shown, the normalized normal and shear stresses are all identically matching with the reported data in the literature, which are solved both analytically and using finite element methods as reported in Dragoni and Goglio.^[2] This demonstrates that the current solution approach successfully solves the equation set. Because the model developed is an analytical model, with the added internal pressure and thermal stress treated as boundary

**Figure 4.** Comparison of the normalized stress field with the Lubkin-Reissner^[1] solution and Goglio-Paolino solution^[23] using the input conditions given in Table 1.

conditions that only change the constants in the differential equation sets with otherwise the same order and coefficients of the unknown variables, the developed analytical model and its solution procedure are equally valid.

3.2. Setup of parametric case studies

Using a modeling framework developed and validated, the stresses in tube-to-tube adhesive joints are studied for practical operating parameters occurring in HVAC systems. There are various possible combinations of material and geometries for different such applications. A representative example joint is selected matching the geometry of the joints tested in a previously experimental study^[24] to carry out parametric studies and understand the influence of key parameters on the joint performance. The first case study focuses on the adhesive geometric design, namely, the overlap bonding length and adhesive layer thickness, which are important parameters to determine before using adhesive bonds in manufacturing processes. Note that the pressure and temperature effects are not considered during this initial variation of the geometric sizing. After these geometric variations are explored, a second case study investigates the effect of thermal expansion on the stress and strain fields.

The baseline case is defined in Table 3, where the geometric parameters are measured from the actual joints and the material properties of the adhesive (3 M DP420) are collected from the manufacturer's data. Note that E_a and G_a of the selected adhesives were not available, and so the manufacturer suggested a similar alternative adhesive (3 M DP460) having these properties available from experimental measurements; these properties will provide similar trends and guidance on the application of adhesives for HVAC&R system joints. The adherend is made of copper, which is the most common material used for tubes in HVAC&R systems.

An internal pressure of 30 bars is selected based on the operating pressure of typical HVAC&R systems using common refrigerants. The external pressure is set to be 1 bar as atmospheric pressure. Among these common refrigerants, R410A has a relatively high operating pressure of ~30 bar (~435 kPa) at the compressor discharge. There are other refrigerants that operate at much higher pressures (e.g., CO₂), but these require a corresponding tube material with higher strength (e.g., stainless steel). The loading boundary conditions are

Table 3. Baseline geometric sizes, material properties, and loading conditions of the adhesive joint characterized in this study.

Parameters	r_1 (mm)	r_2 (mm)	r (mm)	t (mm)	t_1 (mm)	t_2 (mm)	l (mm)
Values	9.1186	9.9514	9.545	0.1	0.8128	0.8128	4
Parameters	E_1 (GPa)	E_2 (GPa)	ν_1 (-)	ν_2 (-)	E_a (MPa)	G_a (MPa)	α (1/K)
Values	117.2	117.2	0.33	0.33	2135	375	1.7×10^{-5}

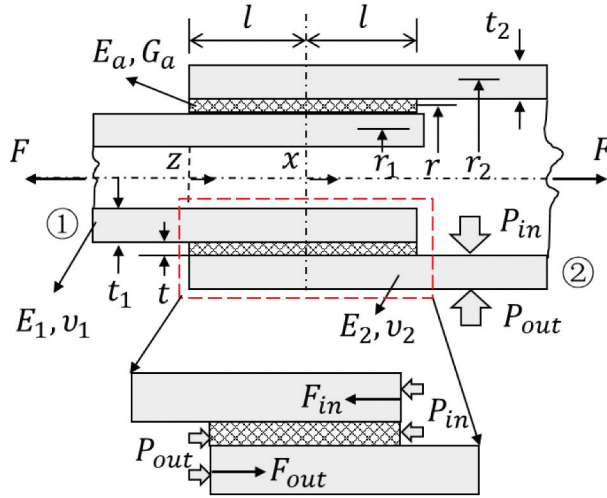


Figure 5. HVAC&R adhesive tube-to-tube joint axial force balance with pressure difference across the tubes.

defined specifically for joints in HVAC&R systems that are usually not structural parts and do not have a large external force applied.

Figure 5 shows the force balance in the axial direction with the pressure difference across the tubes. The main purpose of these joints is to connect components without leakage under the operating pressure. Thus, in the parametric case studies, the axial force is calculated based on the pressure difference acting on the tubes in the axial direction.

$$\begin{aligned}
 F_{out} &= P_{out} \times \pi \left(\left(r_2 + \frac{t_2}{2} \right)^2 - \left(r - \frac{t}{2} \right)^2 \right) \\
 F_{in} &= P_{in} \times \pi \left(\left(r + \frac{t}{2} \right)^2 - \left(r_1 - \frac{t_1}{2} \right)^2 \right)
 \end{aligned} \tag{32}$$

Nevertheless, in some applications, there may be a different external force on these joints (e.g., if they are load-bearing) in the system, and the generality of the model would allow for the same analysis as long as the force is along the axial direction. In such a case where an additional external force needs to be considered, it can be trivially added as:

$$F = F_{in} - F_{out} \tag{33}$$

3.3. Influence of adhesive bonding overlap length and thickness

For tube-to-tube joints, there are two critical adhesive dimensions that need to be determined for a given tube size and materials: the bonding overlap length ($2l$) and adhesive thickness (t). The bonding overlap length $2l$ is first varied over a viable range from 2 mm to 16 mm (compared to the baseline of 8 mm), while the rest of the parameters are kept the same. The predicted stress distribution in the adhesive layer is plotted along the previously defined dimensionless axial coordinate variable z in Figure 6.

It is observed that two peak stresses appear at both ends of the adhesive with the maximum stress at location $z = 0$. Decreasing the bonding length significantly increases both the maximum shear and normal stresses in the adhesive layer. The normal stress profile changes with the bonding length, while the shear stress profile stays relatively consistent in shape. With decreasing the length, comparing $l = 4$ mm with $l = 2$ mm, two local minima move to the center point and merge as one global minimum, and the compressive stress becomes largest at the center point.

In this situation where the joints are not load-bearing components, with relatively high internal pressure (30 bars), the magnitude of these stresses is very low compared to the adhesive strength (usually >20 MPa). Therefore, static loading failure is not a concern for normal operating pressures. In the case of external loading where static failure might be a concern, the length should be selected such that the maximum stress is smaller than the allowed material strength for both normal and shear stress.

The influence of adhesive bondline thickness (t) is studied next while keeping the rest of the geometric parameters constant. Note that the model assumes that the adhesive is a thin layer without considering bending, which limits the applicability of thick adhesive layers. In general, for epoxy-type adhesives, a thin layer is always recommended by the manufacturer due to the fact that epoxies have been shown to have higher shear strength in standardized testing with relatively thin layers (da Silva et al., 2006). Also, a thicker bondline may have more voids and pre-cracking in the manufacturing process. For example, for DP420 the manufacturer-recommended bondline thickness is in the range of 0.1 mm to 0.2 mm. Thus, the thickness t is varied from 0.06 mm to 0.2 mm in the parametric case study (where the value of 0.1 mm is the baseline). In the simulation results, shown in Figure 7, both normal and shear stresses stay relatively constant with changing bondline thickness; the effect of thickness is much less significant compared to the bonding length. In practice, these results suggest that the manufacturer recommendation for bondline thickness should be followed.

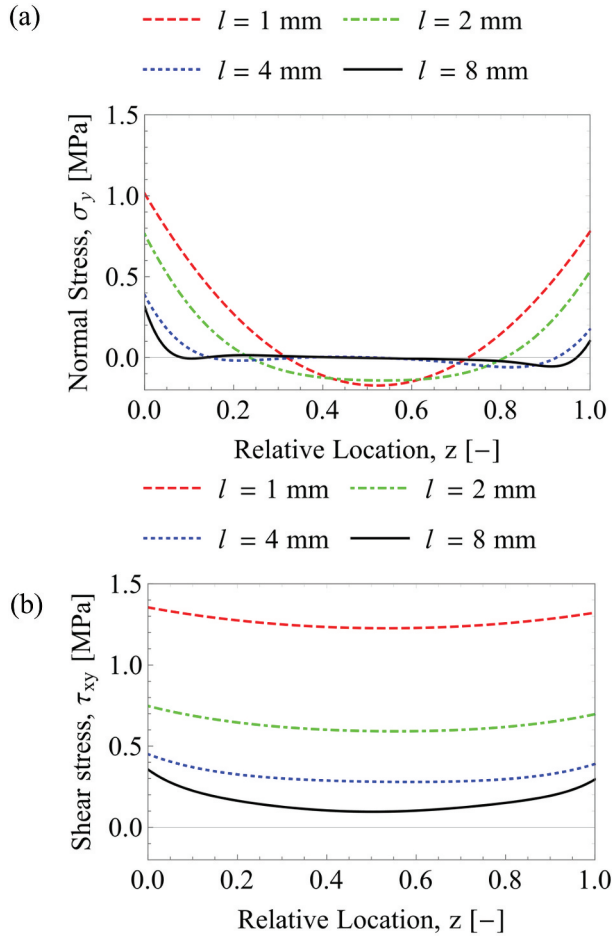


Figure 6. Variation of stress distributions in the adhesive layer with the change of bonding overlap length ($2l$) plotted against the dimensionless variable z : (a) normal stress; and (b) shear stress.

3.4. Influence of thermal expansion

Robustness under repeated thermal expansion and contraction is key to joint reliability in HVAC&R applications. Large temperature changes are expected to occur periodically throughout the life of the system as it cycles on/off or changes operating conditions. The current model adds thermal strain due to the thermal expansion such that it can capture the influence of temperature change on the stress fields in the adhesive layer.

Based on the common operating conditions in HVAC&R systems, the change in temperature varies from $\Delta T = -100\text{K}$ to $+100\text{K}$. An absolute temperature change of 100 K is an extreme case that would only happen in some start-up and shutdown operations of the system. A positive temperature change indicates an increase in the temperature compared to the initial temperature, while a negative change indicates a decrease. It is important to

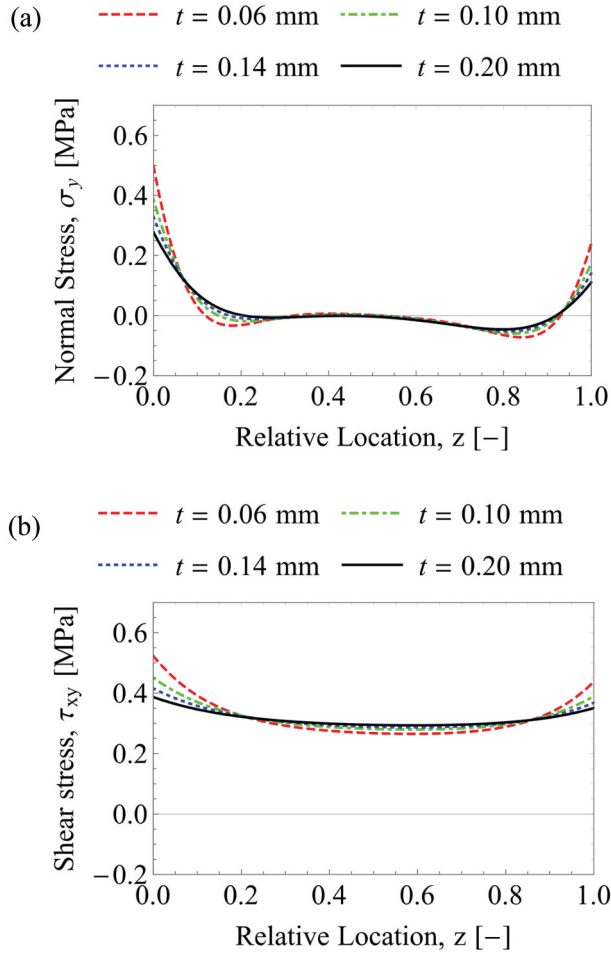


Figure 7. Variation of stress distributions with the change of adhesive thickness (t) while keeping the axial force constant. The results are plotted against the dimensionless variable z : (a) normal stress; (b) shear stress.

consider this when dealing with joints in different locations of the systems. For example, considering a vapor compression system working at room temperature, the joints on the condensing side will usually experience a positive temperature change, while the joints on the evaporating side will see a negative temperature change.

The effect of a temperature change on the stress distributions in the adhesive layer is shown in Figure 8. Comparing Figure 8 with Figure 6, first note the very different scales for vertical axes showing the magnitude of the stress. The thermal-expansion-induced stresses are significantly larger compared to the contribution of the internal pressure to the stress field. Due to the symmetries in the joint, the thermal-expansion-induced stress fields are centrosymmetric around $z = 0.5$, and both normal and shear stress values at

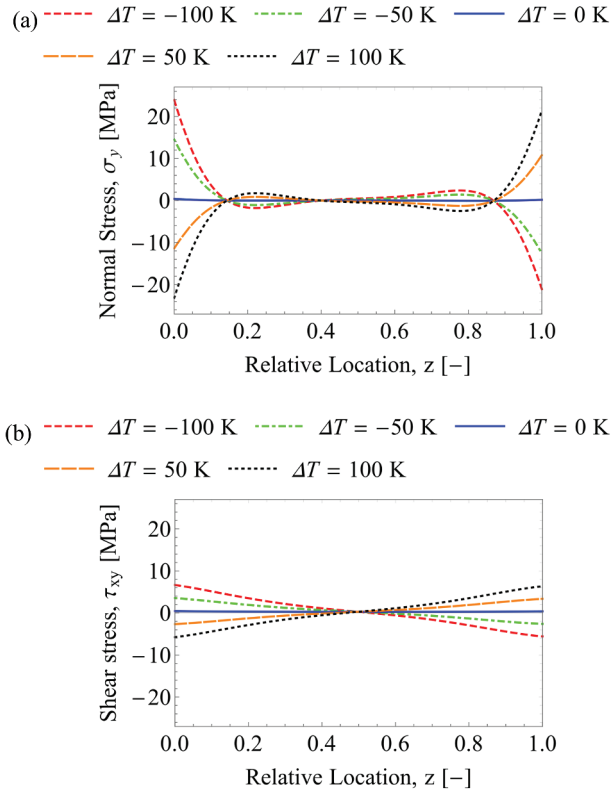


Figure 8. Variation of stress distributions in the adhesive layer with a change of temperature ($\Delta T = -100$ K to $+100$ K) plotted against the dimensionless variable z : (a) normal stress; and (b) shear stress.

$z = 0$ that do not change with temperature. Moving away from the center ($z = 0.5$) towards both ends ($z = 0$ and $z = 1$), thermal expansion has an increasing impact on the stress distributions such that the peak stresses appear at both ends. These maximum stresses increase as the change in temperature becomes larger (such as from 50 K to 100 K in the results shown here). It is worth noting that for positive temperature changes, positive values for both stresses appear at location $z = 1$ and negative values for both stresses appear at $z = 0$. A negative temperature change has the opposite influence on the stress fields; however, the maximum and minimum stresses are not exactly the same with opposite temperature changes due to the pre-existing stress fields from axial loading. This behavior is expected as the expansion versus contraction has opposite impacts on the thermal strain. Overall, the magnitude of the stresses is very sensitive to only small changes in temperature.

Note that the stresses will be different if the joints are used as load-bearing structures. In the previous results shown in [Figure 6](#) and [Figure 8](#), the axial force is calculated using Eqn. (32) and Eqn. (33) with the parameters given in

Table 4. Normal and shear stresses at both ends of the joints under various axial forces and temperature changes.

F (N)	152			5000		
ΔT (K)	-50	0	+50	-50	0	+50
$\sigma_{z=0}$ (MPa)	12.1	0.39	-11.4	24.5	12.7	0.94
$\sigma_{z=1}$ (MPa)	10.5	0.17	10.8	-4.9	5.7	16.3
$\tau_{z=0}$ (MPa)	3.5	0.45	-2.6	17.9	14.8	11.7
$\tau_{z=1}$ (MPa)	-2.6	0.39	3.4	9.8	12.8	15.8

Table 3. The axial force due to the internal pressure is only 152 N. A heavily loaded case with an axial force of 5,000 N is presented to further illustrate the major influence of the thermal stresses at an intermediate temperature change of $\Delta T = \pm 50K$, which is realistic and common in HVAC&R systems such as in ice makers or frozen storage applications. A summary of the peak stresses at both ends of the adhesive joint for low (152 N) and high (5,000 N) axial loads is shown in **Table 4** with temperature changes from -50 K to $+50$ K.

Recall that these stresses have two sources, namely, the axial-force-induced stress and thermal-expansion-induced stress. At low axial force ($F = 152$ N), the thermal stresses dominate the stress profile with respect to the baseline (0 K); the baseline axial stresses induced by pressure alone are close to zero. It requires a very high axial force ($F = 5,000$ N) before both the axial force and thermal stress play important roles.

The thermal stresses together with axial force loading can create complicated stress distributions. It can be noticed that the maximum normal and shear stresses have different values and locations after experiencing temperature change. To explain this, several values in **Table 4** deserve special attention. For example, at $F = 150$ N and $\Delta T = 50$ K, the normal stress at $z = 0$ is 12.1 MPa, which is similar to the normal stress at the same location at $F = 5,000$ N and $\Delta T = 0$ K. A 50 K temperature change can induce the same amount of stress at the same location as an axial force of 5,000 N. Depending on the loading condition and location within the adhesive, the thermal stress can significantly increase the maximum stress, which is especially critical with pre-existing loading as shown in **Table 4**. At $F = 5,000$ N and $\Delta T = -50$ K, the normal stress at $z = 0$ reaches a very high value of 24.5 MPa, which doubles the value when considering the thermal stress and is close to the safe limit on shear stress for some adhesives. Both the positive and negative temperature changes, as well as the direction of the external loading conditions, must therefore be carefully considered in the system design phase.

3.5. Discussion

The above analyses clearly show that, in adhesive tube-to-tube joints, thermal-expansion-induced stresses play a critical role in determining the overall stress

distribution. Variations in joint temperatures can significantly change the stress distribution. In HVAC&R systems, these large temperature swings will occur frequently with typical system operations. Thermal stress and strain must be included in the stress analysis.

Note that additional model validation should be conducted through experimental investigation as future work. The usefulness of this analytical model depends on whether the applied boundary conditions are realistic reflections of what would occur in adhesive joints in HVAC&R applications. This can only be investigated with experimental measurements of the stress and strain in the joints within these applied settings for subsequent comparison to the model predictions.

Fatigue failure can occur with stress cycling at values much lower than the static strength limit. If the system experiences temperature cycling, these thermally induced stresses will appear cyclically. The most accurate method to predict the failure of adhesives is the evaluation of crack initiation and crack propagation. However, the material behavior of adhesives, especially the fatigue crack growth, must be obtained using costly and time-consuming experiments. For example, the cohesive zone model requires accurate measurements to define the traction-separation behavior. It is extremely difficult to measure some of the required input parameters such as the initial displacement δ_0 , failure displacement δ_f , and fracture toughness G , which are not readily available properties for many adhesives. It is also critical to check that no pre-existing defect below the detectable size will grow during the lifetime of the joints, further complicating this approach. Alternatively, the model framework developed here can be combined with damage growth methods such as Paris' Law, where the needed input parameters, $\Delta\sigma_{y,max}$ and $\Delta\tau_{xy,max}$ under cyclic temperature changes,^[25] can be retrieved from the model to provide guidance for reliability design for thermal fatigue without exhaustive testing.

4. Summary and conclusions

In this study, an analytical model for predicting normal and shear stress distributions in the adhesive layers of tube-to-tube adhesive joints is developed, validated, and applied to parametric case studies. A classical model for this situation is modified to add the influence of thermal expansion and contraction, which is necessary due to the constantly changing temperatures in HVAC&R systems. A solution process using Laplace transforms is implemented to provide an explicit closed-form solution. The solution is validated against published data from the literature, and an exact match is achieved.

Applying the developed model to tube-to-tube joints, the relation between the joint stress and strain distributions and critical geometric and operating parameters was probed. In particular, parametric case studies investigated the

influence of the adhesive overlapping length, adhesive bondline thickness, and temperature change experienced by the joints. Several key conclusions can be drawn:

- The peak stresses usually appear at both ends of the adhesive where failure may happen. Decreasing the bonding length will largely increase the maximum stress for both the shear and normal stresses in the adhesive layer. On the contrary, adhesive layer thickness plays a less important role in determining the stress fields and the manufacturer recommended thickness should be followed.
- Thermally induced expansion and contraction play a critical role in the determination of the stress distributions of adhesive joints, especially in HVAC&R systems that will have large temperature swings. Based on the existing loading, even a small temperature change can cause significant stresses. The positive and negative temperature changes should be considered individually. From both static and fatigue failure perspectives, thermal expansion must be considered in the joint stress analysis.

In summary, this paper reports the first tube-to-tube adhesive joint model of stress and strain distributions aiming to consider the working conditions of HVAC&R applications. All of these results provide a detailed guidance for the use of adhesive joints across different applications and locations in HVAC&R systems. The model serves as a framework to evaluate and compare the performance of different adhesives, as long as the adhesive properties can be determined as inputs.

Acknowledgements

The authors would like to thank Prof. Ganesh Subbarayan for his help and guidance in the model development.

Disclosure statement

No potential conflict of interest was reported by the author(s).

References

- [1] Lubkin, J. L.; Reer, E. Stress Distribution and Design Data for Adhesive Lap Joints between Circular Tubes. *Trans. ASME*. 1956, 78, 1213–1221. <https://doi.org/10.1115/1.4013993>.
- [2] Goglio, L.; Dragoni, E. Adhesive Stresses in axially-loaded Tubular Bonded joints—Part I: Critical Review and Finite Element Assessment of Published Models. *IJAA*. 2013, 47, 35–45. <https://doi.org/10.1016/j.ijadhadh.2013.09.009>.

- [3] Terekhova, L. P.; Skoryi, I. A. Stresses in Bonded Joints of Thin Cylindrical Shells. *Strength Mater.* 1972, 4, 1271–1274. <https://doi.org/10.1007/BF01527977>
- [4] Pugno, N.; Carpinteri, A. Tubular Adhesive Joints under Axial Load. *J. Appl. Mech.* 2003, 70(6), 832–839. <https://doi.org/10.1115/1.1604835>.
- [5] Shi, Y. P.; Cheng, S. Analysis of adhesive-bonded Cylindrical Lap Joints Subjected to Axial Load. *J. Eng. Mech.* 1993, 119, 584–602. [https://doi.org/10.1061/\(ASCE\)0733-9399\(1993\)119:3\(584\)](https://doi.org/10.1061/(ASCE)0733-9399(1993)119:3(584)).
- [6] Nayeb-Hashemi, H.; Rossettos, J. N.; Melo, A. P. Multiaxial Fatigue Life Evaluation of Tubular Adhesively Bonded Joints. *IJAA.* 1997, 17, 55–63. [https://doi.org/10.1016/S0143-7496\(96\)](https://doi.org/10.1016/S0143-7496(96)).
- [7] Nemeş, O.; Lachaud, F.; Mojtabi, A. Contribution to the Study of Cylindrical Adhesive Joining. *IJAA.* 2006, 26, 474–480. <https://doi.org/10.1016/j.ijadhadh.2005.07.009>.
- [8] Nemeş, O.; Lachaud, F. Modeling of Cylindrical Adhesively Bonded Joints. *J. Adhes. Sci. Technol.* 2009, 23, 1383–1393. <https://doi.org/10.1163/156856109X432983>.
- [9] Kumar, S. Analysis of Tubular Adhesive Joints with a Functionally Modulus Graded Bondline Subjected to Axial Loads. *IJAA.* 2009, 29, 785–795. <https://doi.org/10.1016/j.ijadhadh.2009.06.006>.
- [10] Kumar, S.; Scanlan, J. P. Stress Analysis of shaft-tube Bonded Joints Using a Variational Method. *J. Adhes.* 2010, 86, 369–394. <https://doi.org/10.1080/00218461003704329>.
- [11] Martinez, M. A.; Velasco, F.; Abenojar, J.; Pantoja, M.; Del Real, J. C. Analytical Solution to Calculate the Stress Distribution in pin-and-collar Samples Bonded with Anaerobic Adhesives (Following ISO 10123 Standard). *IJAA.* 2008, 28, 405–410. <https://doi.org/10.1016/j.ijadhadh.2008.04.007>.
- [12] Hart-Smith, L. J. Further Developments in the Design and Analysis of adhesive-bonded. *ASTM special technical publications.* 1981, 3. <https://doi.org/10.1520/STP33472S>.
- [13] Chon, C. T. Analysis of Tubular Lap Joint in Torsion. *J. Compos. Mater.* 1982, 16(4), 268–284. <https://doi.org/10.1177/002199838201600402>.
- [14] Thomsen, O. T.; Kildegaard, A. Analysis of Adhesive Bonded Generally Orthotropic Circular Shells. Developments in the Science and Technology of Composite Materials, Proceedings of the Fourth European Conference of Composite Materials, 1990; 723–729.
- [15] Lee, D. G.; Kim, K. S.; Lim, Y. T. An Experimental Study of Fatigue Strength for Adhesively Bonded Tubular Single Lap Joints. *J. Adhes.* 1991, 35, 39–53. <https://doi.org/10.1080/00218469108030434>.
- [16] Lee, S. J.; Lee, D. G. Development of a Failure Model for the Adhesively Bonded Tubular Single Lap Joint. *J. Adhes.* 1992, 40, 1–14. <https://doi.org/10.1080/00218469208030467>.
- [17] Kinloch, A. J.; Guild, F. Predictive Modeling of the Properties and Toughness of rubber-toughened Epoxies. In *Toughened Plastics II, Novel Approaches in Science and Engineering*, Riew, C. K., Kinloch, A. J. Eds. USA: Advances in Chemistry Series Publications, 1996; pp. 1–25. <https://doi.org/10.1021/ba-1996-0252.ch001>
- [18] Adams, R. D.; Comyn, J.; Wake, W. C., *Structural Adhesive Joints in Engineering*; Chapman & Hall: London, United Kingdom, 1997.
- [19] Alwar, R. S.; Nagaraja, Y. R. Elastic Analysis of Adhesive Butt Joints. *J. Adhes.* 1976, 7(4), 279–287. <https://doi.org/10.1080/00218467608075059>.
- [20] Yadagiri, S.; Papi Reddy, C.; Sanjeeva Reddy, T. Viscoelastic Analysis of Adhesively Bonded Joints. *Comp. Struct.* 1987, 27(4), 445–454. [https://doi.org/10.1016/0045-7949\(87\)90275-6](https://doi.org/10.1016/0045-7949(87)90275-6).
- [21] Adams, R.; Peppiatt, N. Stress Analysis of Adhesive Bonded Tubular Lap Joints. *J. Adhes.* 1977, 9, 1–18. <https://doi.org/10.1080/00218467708075095>.
- [22] Kumar, S.; Pandey, P. C. Fatigue Life Prediction of Adhesively Bonded Single Lap Joints. *IJAA.* 2011, 31(1), 43–47. <https://doi.org/10.1016/j.ijadhadh.2010.10.002>.

- [23] Goglio, L.; Paolino, D. Adhesive Stresses in axially-loaded Tubular Bonded joints–part Ii: Development of an Explicit closed-form Solution for the Lubkin and Reer Model. *IJAA*. 2014, 48, 35–42. <https://doi.org/10.1016/j.ijadhadh.2010.10.002>.
- [24] Liu, H.; Geoghegan, P. J.; Weibel, J. A.; Ziviani, D.; Groll, E. A. Proof-of-concept Testing of Adhesive Joints for HVAC&R Applications, 13th IEA Heat Pump Conference, Jeju, Korea, April 26-29, 2021, 332.
- [25] Kinloch, A. J.; Osiyemi, S. O. Predicting the Fatigue Life of Adhesively-Bonded Joints. *J. Adhes.* 1993, 43(1–2), 79–90. <https://doi.org/10.1080/00218469308026589>.